UNDERSTANDING THE ROLE OF MK-STYX IN STRESS RESPONSE PATHWAYS USING COMPUTATIONAL MODELING OF ITS CRYSTAL STRUCTURE

Emma Marie Wilber Hepworth
Department of Biology, College of William & Mary
Advisor: Shantá D. Hinton, Ph.D.

Abstract

The pseudophosphatase MK-STYX [MAPK (mitogen-activated protein kinase) - phosphoserine/threonine/tyrosine-binding protein] is an atypical noncatalytically active MKP (MAPK phosphatase). The DUSP (dual-specificity phosphatase) domain of MK-STYX lacks critical histidine and cysteine residues in the active site motif (HCX_5R), rendering it inactive. MK-STYX also contains a CH2 domain (cell division cycle 25 phosphatase homology 2 domain) interrupted by a KIM (kinase interacting motif). Unlike the KIM of its MKP active homologs, MK-STYX lacks the consecutive arginines necessary to bind MKP target proteins. Despite this, MK-STYX has been shown to be a regulator of multiple pathways such as stress response, apoptosis, and neurite formation, and has been implicated in various cancers. Uncovering the macromolecular structure of MK-STYX is the key to understanding the atypical domains of MK-STYX, the mechanisms they use to carry out their role in signaling pathways and induce particular phenotypes, and how this differs from the other MKPs. Determining the structure of MK-STYX requires a combined approach of protein crystallography and bioinformatics. An investigation using computational approaches revealed that the lack of consecutive arginines in the KIM of MK-STYX results in a different predicted binding pocket compared to that of active homologs, supporting the idea that MK-STYX has a unique function.

Introduction

Within each cell, communication is key to ensuring smooth operation. Nowadays, people have many ways to communicate with their coworkers, friends, and family, to carry out projects, coordinate plans, and remain abreast of important events. Similarly, cells have numerous ways in which they "talk", both within the cell and with others, using signaling pathways[1]. One important messenger is the phosphate molecule, which when added (through phosphorylation) or removed (through dephosphorylation) from a protein can change the shape and function of that protein[2]. The processes of phosphorylation and dephosphorylation are highly regulated within the cell in order to maintain homeostasis. Two kinds of proteins have the vital job of maintaining this delicate balance, kinases, which are responsible for phosphorylation, and phosphatases, which are responsible for dephosphorylation[2].

While enzymes such as kinases and phosphatases are essential to proper cell function, there are also proteins known as "pseudoenzymes" that play an important cellular role[3]. These proteins are catalytically inactive homologs of enzymes such as: kinases, phosphatases, proteases, synthetases, etc. Pseudoenzymes are highly conserved evolutionarily and an estimated 10% of the proteins encoded in the human genome are pseudoenzymes[1,4,5]. However, their biologic role remains elusive. While these proteins were previously thought to be "dead" enzymes with no unique cellular functions, they are receiving more attention over the last decade as researchers uncover new information that reveals a fascinating and complex area of study[1,3,5–7]. One such protein of interest is the pseudophosphatase MK-STYX [MAPK (mitogen-activated protein kinase)-

phosphoserine/threonine/tyrosine-binding protein], also called DUSP-24 (dual-specificity protein phosphatase 24) or STYXL1 (Serine/threonine/tyrosine-interacting-like protein 1)[8–10].

MK-STYX is a catalytically inactive PTP (protein tyrosine phosphatase) and the only catalytically inactive member of the mammalian MKP (MAPK phosphatase) subfamily of DUSPs (dual-specificity phosphatases)[9–11]. The main function of MKPs is to dephosphorylate target kinases, MAPKs/ERKs (extracellular signal regulated kinases), in order to regulate MAPK/ERK signaling pathways[12,13]. MKPs carry out this function using two conserved domains, an N-terminal noncatalytic binding domain and a C-terminal catalytic domain (DUSP domain)[12]. The N-terminal noncatalytic domain determines substrate specificity and is responsible for recognizing and binding the target MAPK/ERK[12–14]. The C-terminal catalytic domain removes a phosphate group from the MAPK/ERK.

PTPs have a highly conserved signature active site motif consisting of histidine and cysteine, followed by any five amino acids, and then an arginine (HCX_5R)[15–18]. This is the region of the protein that catalyzes the removal of a phosphate from the substrate. However, the active site of MK-STYX has the sequence FSTQGISR (containing phenylalanine and serine), which lacks the critical histidine and cystine residues and renders MK-STYX catalytically inactive[1,9,10]. The inactive DUSP domain in MK-STYX is also referred to as a "STYX" domain, after the prototypical pseudophosphatase STYX (serine/threonine/tyrosine-binding protein), classifying MK-STYX as a STYX domain PTP[19–21].

In addition to an atypical C-terminal catalytic domain, MK-STYX has an atypical N-terminal domain[10]. Typical MKPs have a N-terminal noncatalytic domain composed of a CH2 domain (cell division cycle 25 phosphatase homology 2 domain) interrupted by a KIM (kinase-interacting motif)[12]. This noncatalytic domain is used for substrate recognition and docking of the target at the KIM, allowing the DUSP domain to then remove the phosphate group[13]. However, MK-STYX lacks the two to three consecutive arginine residues in its KIM that are necessary to dock MAPKs/ERKs[10,12].

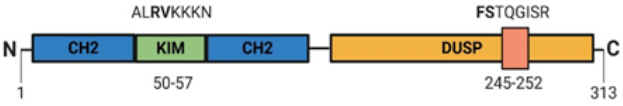

Figure 1: Diagram of the Domains and Key Regions of MK-STYX. Image created with BioRender.

Figure 1 displays a schematic diagram of MK-STYX, showing the arrangement of the N-terminal noncatalytic domain and the C-terminal catalytic domain, along with the location of key atypical regions within these domains. Table 1 compares critical sequences within the KIM and active site of MK-STYX with those of its active homologs, MKP-1 (DUSP-1) and MKP-3 (DUSP-6)[10,13,22].

	KIM	Active Site Motif
Consensus Sequence	X I X L R R X K K G	H C X X X X X R
MKP-1	T I V R R R A K - G	H C Q A G I S R
MKP-3	G I M L R R L Q K G	H C L A G I S R
MK-STYX	I T A L R V K K K N	F S T Q G I S R

Table 1: Table Comparing the Sequences of MK-STYX and its Active Homologs at the KIM and Active Site Motif

Given that the domains of MK-STYX lack the conserved functions of its active homologs, it would be easy to assume that MK-STYX has lost its overall protein function. However, while MK-STYX may not function in the same way as a typical MKP, it is very much still a functioning protein with an important role in cellular pathways. MK-STYX has been implicated in apoptosis pathways, stress granule formation, neurite formation, and as a promoter of oncogenesis and malignancy in glioma and hepatocellular carcinoma[1,9,23–26].

In previous studies, MK-STYX has demonstrated the ability to regulate various signaling pathways[1,10]. The overexpression of MK-STYX in PC-12 cells induced neurite formation through the RhoA signaling pathway[27–29]. A homozygous missense mutation in the *STYXL1* gene leads to a version of MK-STYX with a P311A mutation, known as MK-STYX$_{\text{ID (intellectual disability)}}$, that has been linked to a family with a history of developmental delays, intellectual disability, and early onset epilepsy[30]. Within the last couple of years, MK-STYX has been implicated as a possible regulator in the oncogenesis pathways of glioma and hepatocellular carcinoma[25,26].

Perhaps the role of MK-STYX that is best characterized, is its role in stress response pathways. MK-STYX is a regulator of apoptotic signaling by inducing stress-activated mitochondrial-dependent apoptosis by inhibiting the phosphatase PTPM1 (PTP localized to the mitochondrion 1)[1,10,23,24]. Another critical role of MK-STYX in the cellular stress response is the ability of MK-STYX to reduce stress granules (SGs), membraneless organelles that form in the cytosol as a protective response to stressful physiologic conditions[9,31–34]. SGs are untranslated messenger ribonucleoproteins (mRNPs) that are stalled in the translation initiation stage of protein synthesis. While SGs are a protective response to stressful cellular conditions, SGs that persist in the cytosol, instead of being properly cleared, become toxic. Prolonged SGs are linked to neurodegenerative diseases and certain cancers[31,32]. The physiologic conditions that induce SGs can be both physical and chemical, including thermal stress, osmotic stress, and oxidative stress, the latter of which can be induced by a variety of factors such as sodium arsenate and even microgravity[34–38].

The catalytic activity of MK-STYX can be experimentally restored by replacing phenylalanine (position 245) and serine (position 246) with histidine and cysteine residues, respectively, to create a catalytically active mutant (MK-STYX$_{\text{active mutant}}$) that has the PTP active site motif (HCX_5R) restored[9,39]. Interestingly, MK-STYX$_{\text{active mutant}}$ does not retain the ability to reduce SGs, both those induced by G3BP-1 [Ras-GAP (GTPase-activating protein) SH3 (Src homology 3) domain-binding protein-1] and endogenous SGs[1,9]. Actually, the opposite effect is seen and MK-STYX$_{\text{active mutant}}$ increases the size of G3BP-1-induced SGs.

Interest in pseudophosphatases and the funding of relevant studies has historically been limited due to misconceptions about the unimportance of "dead" enzymes[10]. For this reason, the mechanisms used by MK-STYX to induce these effects are not well understood. An essential step towards elucidating the role of MK-STYX in stress response pathways is to determine its macromolecular structure.

Determination of Macromolecular Structures

Experimental Approaches

Determining the macromolecular structure of a protein is an important step towards understanding the unique relationship between structure and function in that protein[13,40]. Knowing the structure leads to uncovering the molecular mechanisms of the protein. It also allows for the development of drugs to target the protein if it is involved in disease pathways. Traditional approaches for structure determination include: X-ray crystallography, nuclear magnetic resonance (NMR) spectroscopy, and electron microscopy (cryo-EM and 3D-EM). These methods use different types of experimental data to determine the overall macromolecular structure of a protein. X-ray crystallography uses the data from the X-ray diffraction pattern, NMR uses the distance between atoms, and EM uses images of individual molecules[41–44].

Full or partial structures have already been determined for the active homologs of

MK-STYX, MKP-1[40] and MKP-3[13,22], and for the prototypical pseudophosphatase STYX[45]. The structure of the catalytic domain of MKP-1 was determined using X-ray crystallography and revealed that the protein is able to bind both phosphorylated tyrosine and threonine side chains because it has a shallow active site[22]. Two partial structures for MKP-3 are known, that of the C-terminal catalytic domain and of the N-terminal domain[13,40]. The structure of the N-terminal domain, also referred to as the ERK2 binding (EB) domain, of MKP-3 was determined using NMR spectroscopy[13]. The structure showed that binding of ERK2 is required for activation of MKP-3 because it induces a conformational change of the C-terminal catalytic domain, revealing that the two domains are functionally coupled. MKP-1 and MKP-3 are examples of how elucidating the macromolecular structure of a protein is a critical step in understanding the function of the protein and the novel mechanisms utilized to carry out its role in cellular pathways.

Computational Approaches

Bioinformatics, defined as "the application of computational tools to organize, analyze, understand, visualize and store information associated with biological macromolecules", continues to have an expanding role within the field of structural biology[46,47] Structural bioinformatics can be used to generate *in silico* 3-D models of protein structures using theoretical predictive methods[48–52]. One such approach to generating predictive protein structures is the I-TASSER (Iterative Threading ASSEmbly Refinement) server[53–55]. This server allows a user to submit the primary sequence of a protein of interest, and the server will then predict the structure of the protein by using structural templates from the PDB (protein data bank) and iterative fragment assembly simulations to construct the full-length protein structure. Computational tools such as I-TASSER provide a powerful and valuable resource for determining and exploring the macromolecular structure of a protein, even without a known crystal structure.

Objectives

1. Determine the function of the domains in MK-STYX and how they interact.
2. Uncover the novel mode of action utilized by MK-STYX in signaling pathways by comparing the structure of MK-STYX to MK-STYX$_{\text{active mutant}}$ and also to its active homologs MKP-1 (DUSP-1) and MKP-3 (DUSP-6).

Materials and Methods

The structure of MK-STYX and its variants will be determined and investigated using a combined approach of X-ray crystallography and bioinformatic tools in order to: thoroughly understand the relationship between structure and function of MK-STYX, how the atypical domains of MK-STYX are linked to the mode of action that allows MK-STYX to regulate cellular stress response pathways, and identify the mechanisms utilized by MK-STYX, beyond those used by its active homologs.

X-ray Crystallography

The sequences for MK-STYX, MK-STYX$_{\text{active mutant}}$, truncated versions of MK-STYX (MK-STYX$_{\text{CH2 truncate}}$ and MK-STYX$_{\text{DUSP truncate}}$), and MK-STYX$_{\text{ID}}$, were each cloned into a pET28a vector containing a polyhistidine sequence (His-tag), a kanamycin resistance gene, and a T7 promoter (GenScript)[56]. Competent *Escherichia coli* containing a DE3 recombinant phage, which encodes for the inducible T7 RNA polymerase, were then transformed with one of the previously mentioned plasmids and grown overnight on kanamycin treated LB-agar plates.

The next day a colony was selected from the plate and grown overnight in LB liquid medium in a shaking incubator. On the following day, the overnight culture was used

Approach	Description	Website
I-TASSER (Iterative Threading ASSEmbly Refinement)[53,54]	Server that uses structural templates from the PDB (Protein Data Bank) to generate the top five predicted models for the structure of a protein and to identify the top ten structural analogs of the predicted protein structure. Also predicts possible functions of the protein using the protein function database BioLip (biologically relevant ligand-protein binding database).	https://zhanglab.ccmb.med.umich.edu/I-TASSER/
MolProbity[57–59]	The purpose of MolProbity is to provide all-atom model validation of macromolecular structures. It analyzes steric hindrance as part of its validation and generates a Ramachandran Plot to show which atom conformations may be sterically disfavored. Another aspect of MolProbity's model validation is analyzing H-bonds and van der Waals energy at atom-atom contacts in order to identify disfavored/impossible overlaps.	http://molprobity.biochem.duke.edu/index.php
PDB (Protein Data Bank)[43]	An archive operated by the RCSB PDB (Research Collaboratory for Structural Bioinformatics PDB) which catalogs the known 3-D macromolecular structures of proteins, DNA, and RNA.	https://www.rcsb.org/
POCASA (Pocket Cavity Search Application)[60]	Probes the surface of a protein with a rolling sphere probe in order to look for pockets (cavities) to predict the location and shape of potential ligand binding sites. These binding sites may indicate a biological function for the protein of interest or a potential drug target.	http://g6altair.sci.hokudai.ac.jp/g6/service/pocasa/
PyMOL Molecular Graphics System[61]	PyMOL is a molecular visualization software that allows the user to visualize PDB files as animated 3-D structures and to manipulate these structures (e.g. through its mutagenesis function) in order to better investigate them. Can also be used to generate and present interactive molecular models.	https://pymol.org/2/

Table 2: Table of Computational Methods

to inoculate fresh LB liquid medium, ranging in volume from 3mL to 1L. These subcultures were incubated with shaking until ready to induce. IPTG (isopropyl β-D-1-thiogalactopyranoside) was added to the cultures to induce expression of the protein of interest and then incubated with shaking at a range of temperatures and for varying durations in order to find the expression conditions that were the most favorable.

Afterwards, the cultures were centrifuged, and the bacterial cell pellets were lysed. Lysates were processed using Nickle resin columns to separate out the His-tagged protein of interest. Protein expression and solubility was analyzed using Western Blots with primary antibodies against both MK-STYX (anti-STYXL1) and the His-tag (His-probe (H-3)).

Due to the COVID-19 pandemic and safety concerns related to in-person lab work, experiments working towards the crystal structure were suspended temporarily and resumed in Fall 2020. The time spent working from home was used to expand on the structural bioinformatics and computational aspects of this project in order to facilitate progress on the objectives. This was done by using I-TASSER (Iterative Threading ASSEmbly Refinement) models and other computational methods (Table 2) to further explore the structure of MK-STYX and gain insight into its function.

Generating Predictive Structures

The amino acid sequence of MK-STYX was submitted to the I-TASSER server[53–55]. I-TASSER generated and reported the top five predicted models of the macromolecular structure of MK-STYX (Figure 2). The models, in PDB file format, were used for further computational analysis.

Binding Pocket Study

MolProbity was used to validate the five structural models of MK-STYX generated by I-TASSER and to determine which of the models was the most sterically favored[57–59]. Model 2 was the model with the best Clashscore and MolProbity score (13.65 and 3.39, respectively). Model 2 was then submitted to POCASA (Pocket Cavity Search Application) to identify and map potential binding pockets on the protein's surface[60]. The crystal structures of the C-terminal catalytic domain for both MKP-1 and MKP-3 were downloaded from the PDB (Protein Data Bank) and submitted to POCASA. Then, the active sites of MK-STYX, MKP-1, and MKP-3 were

visualized in PyMOL with the POCASA-predicted binding pockets overlaid the surface of the respective proteins (Figure 3)[61]. Using surface depictions of the protein made it easier to visualize where the pockets were. They were then visually inspected for structural similarities.

Mutagenesis Study

In order to investigate the significance of the "FS" active site motif in MK-STYX, the "mutagenesis" function in PyMOL was utilized to generate MK-STYX$_{\text{active mutant}}$[61]. Model 2 of MK-STYX (wild-type) was mutated with the following mutations to generate MK-STYX$_{\text{active mutant}}$, F245H and S246C, this generated a catalytically active DUSP domain with the active site motif HCTQGISR. The newly generated MK-STYX$_{\text{active mutant}}$ was submitted to POCASA to identify and map potential binding pockets on the surface of the protein. Using PyMOL, the model of the corresponding protein, either MK-STYX or MK-STYX$_{\text{active mutant}}$, was overlaid with the predicted binding pockets generated by POCASA (Figure 4). The list of identified pockets, the pocket volume, and the pocket Volume Depth (VD) values calculated by POCASA were compared between MK-STYX and MK-STYX$_{\text{active mutant}}$ to see if the protein mutagenesis had changed the number or shape of potential pockets[60].

The same process was used to study the impact of the KIM of MK-STYX lacking consecutive arginine residues. Using the PyMOL mutagenesis function, the KIM of MK-STYX was mutated so that it would have two consecutive arginines by replacing the valine at position 53 with an arginine (V53R). The mutation was done at this particular position in order to make the KIM of MK-STYX more closely resemble the consensus motif, and so that the MK-STYX_V53R mutant has the same arginine arrangement as MKP-3, the active homolog of MK-STYX (Table 1). The MK-STYX_V53R mutant was then submitted to POCASA to identify and map potential binding pockets on the surface of the protein. As mentioned previously, using PyMOL, the model of the corresponding protein, either MK-STYX or MK-STYX_V53R, was overlaid with the predicted binding pockets generated by POCASA (Figure 5). The list of identified pockets, the pocket volume, and the pocket Volume Depth (VD) values calculated by POCASA were also compared between the two proteins to see if the protein mutagenesis had changed the number or shape of potential pockets.

Results

Figure 2 shows the top five predicted models of the structure of MK-STYX, generated by I-TASSER, compared to the known partial structures of its active homologs, MKP-1 and MKP-3, and to the known structure of the prototypical pseudophosphatase STYX. Ribbon depictions were used in order to show secondary structures.

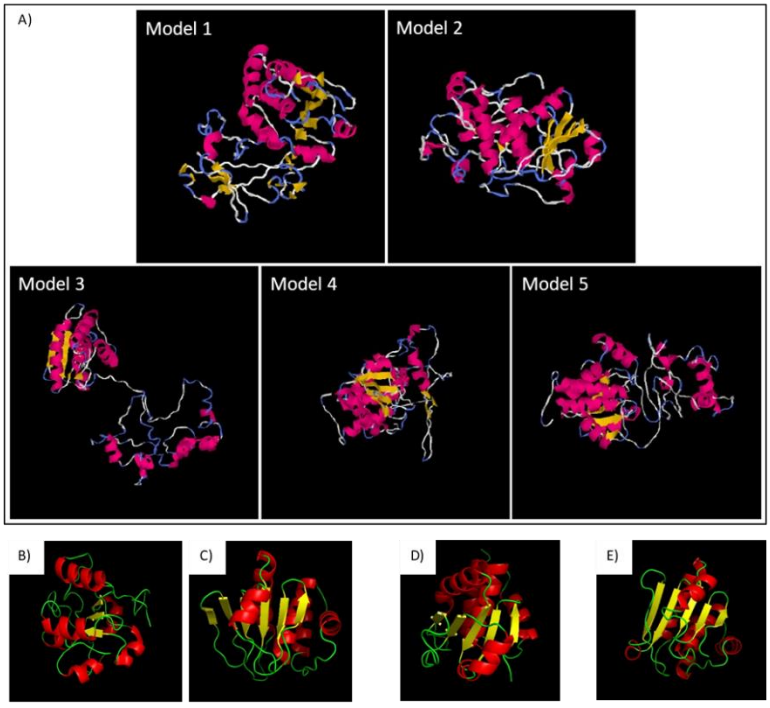

Figure 2: Predicted Structures for MK-STYX Compared to Known Structures of Related Proteins. A) The top five predicted models for the macromolecular structure of MK-STYX, generated by I-TASSER. B) Structure of the N-terminal noncatalytic domain of MKP-3. C) Structure of the C-terminal catalytic domain of MKP-3. D) Structure of the C-terminal catalytic domain of MKP-1. E) Structure of the prototypical pseudophosphatase STYX.

Figure 3 shows the structure and predicted binding pockets of MK-STYX, MKP-1, and MKP-3 with the active site of each protein highlighted in cyan blue. The structures of MKP-1 and MKP-3 show the ligand (sulfate ion for MKP-1 and chloride ion for MKP-3) that was bound to the active site pocket of the respective proteins at the time of crystallography. Surface depictions were used to better show topography of the proteins.

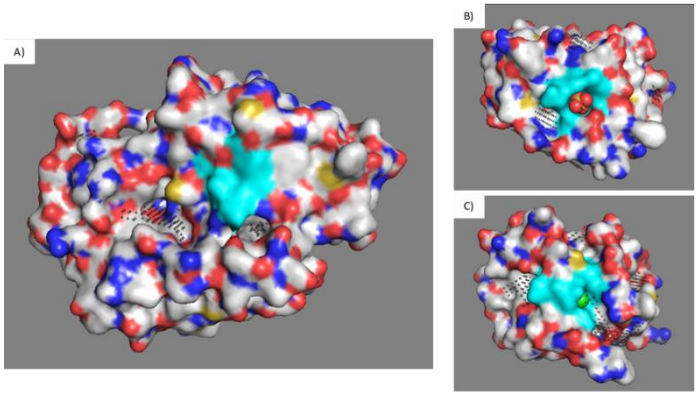

Figure 3: Comparison of the Active Site of MK-STYX (A) with the Active Sites of MKP-1 (B) and MKP-3 (C). Shows the surface diagram of each protein with the active site highlighted in cyan. The small dark "+" marks map the predicted binding pockets on the surface of the protein. A) Surface diagram of MK-STYX. B) Surface diagram of MKP-1 bound to a sulfate ion. C) Surface diagram of MKP-3 bound to a chloride ion.

Figure 4 shows the surface diagrams of MK-STYX and MK-STYX$_{\text{active mutant}}$ overlaid with the respective predicted binding pockets in the area of the active site. No changes to the structure of the active site were observed. Additionally, the volume and VD values of the predicted binding pockets did not change between the two proteins.

Figure 5 shows the surface diagrams of MK-STYX and MK-STYX_V53R overlaid with the respective predicted binding pockets in order to inspect for changes to protein structure or to binding pockets. There was a noticeable change in the shape of one of the predicted binding pockets. The region of interest, including the relevant binding pocket, is outlined by the dashed-line circle. For the MK-STYX_V53R mutant (KIM with two consecutive arginines), the predicted binding pocket in the region of the additional arginine residue in position 53 was smaller than that of MK-STYX (KIM with a single arginine). Also, the respective volume and VD value of the binding pocket decreased from 104 and 242 in MK-STYX (WT) to 89 and 208 in the MK-STYX_V53R mutant.

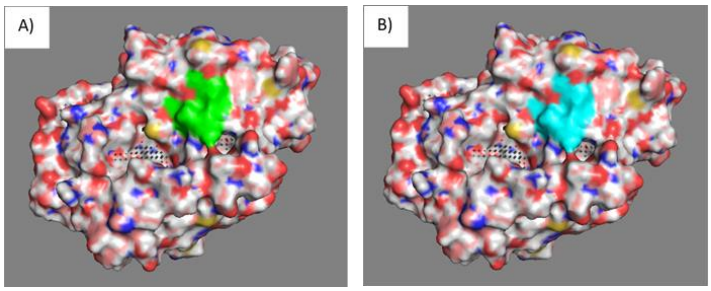

Figure 4: Structure of the Active Site of MK-STYX (A) and MK-STYX$_{\text{active mutant}}$ (B). The small dark "+" marks map the predicted binding pockets on the surface of the protein. A) Surface diagram of MK-STYX (wild-type) with active site (FSX$_5$R) highlighted in green. B) Surface diagram of MK-STYX$_{\text{active mutant}}$ with active site (HCX$_5$R) highlighted in cyan.

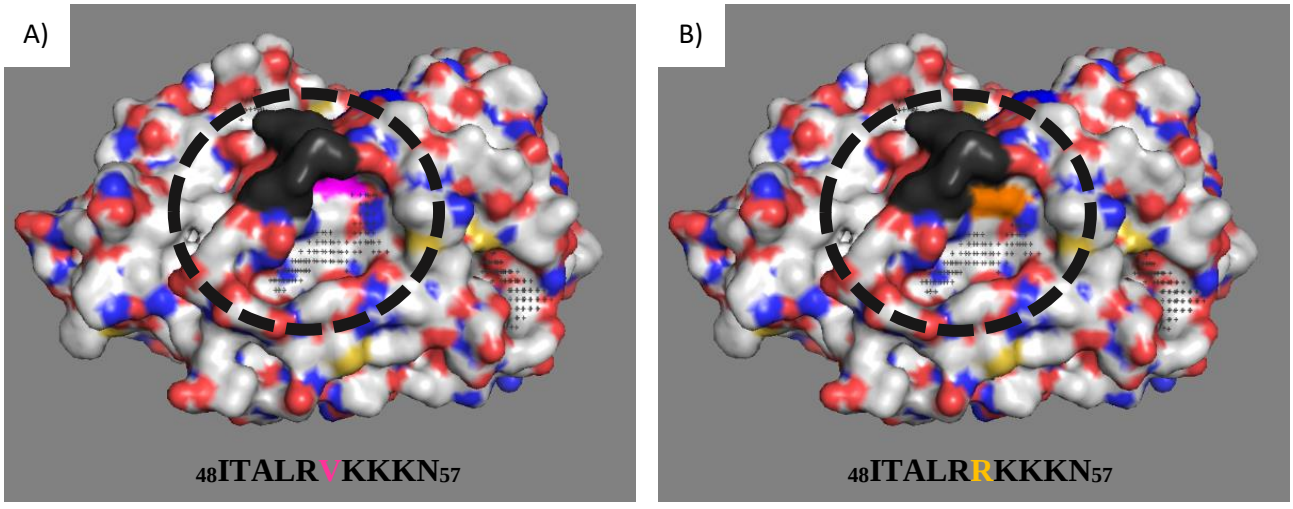

Figure 5: Structure of the KIM of MK-STYX (A) and MK-STYX_V53R mutant (B). The small dark "+" marks map the predicted binding pockets on the surface of the protein. The dashed-line circle outlines the area of interest. A) Surface diagram of MK-STYX (wild-type) with the valine (V) at position 53 highlighted in pink. B) Surface diagram of MK-STYX_V53R mutant with the arginine (R) at position 53 highlighted in orange.

Discussion

Computational models such as I-TASSER have limitations, evidenced by the obvious variation between the top five predicted structures of MK-STYX, and that is why this approach involves both bioinformatics and X-ray crystallography. This combination allows us to evaluate the accuracy of computational methods of structure determination and eventually to strengthen the prediction algorithms once the crystal structure of MK-STYX has been submitted to the PDB. It was difficult to compare the active site of MK-STYX to that of MKP-1 and MKP-3 when MK-STYX is not bound to a ligand. The binding of a ligand induces a conformational change in the active site pocket of MKP-1 and MKP-3. However, it does seem like MK-STYX has a predicted binding pocket on the lower edge of the active site where a ligand could bind, in a similar location to the bound ligands of MKP-1 and MKP-3. This is important information for us to keep in mind during the process of obtaining the crystal structure of MK-STYX. Furthermore, this will provide a region of interest to compare between the predicted structure and crystal structure of MK-STYX. Once the conformation of MK-STYX when bound to a ligand is determined, these structures can be revisited.

The mutagenesis study of the MK-STYX active site aligns with the expectation that pseudophosphatases maintain their 3-D structure, even though they lack catalytic function. This indicates that MK-STYX is able to bind the same substrates in both the wild-type and the active mutant form. The MK-STYX_V53R mutant had its KIM domain mutated so that it contained consecutive arginines in the same position as its active homolog MKP-3. The change in shape and decrease in volume of the binding pocket on MK-STYX_V53R provides evidence that the KIM of MK-STYX may be responsible for binding a unique set of substrates compared to typical MKPs, and more specifically to its active homolog MKP-3. This is further supported by the fact that the CH2 domain is known to regulate the substrate specificity of MKPs. This is exciting evidence that MK-STYX may use a novel mechanism to regulate critical signaling pathways, such as stress response. If this binding site is confirmed by crystallography, it would be an important step in developing drugs that target MK-STYX.

In order to confirm these computational findings, we will continue our work on determining the crystal structure of MK-STYX. Additionally, the use of combined bioinformatic and traditional methods for structure determination, as presented here, will provide a way to assess how computational approaches can be used to study other pseudoenzymes. MK-STYX continues to be linked to an increasing number of signaling pathways and human diseases. Determining the macromolecular structure of MK-STYX is critical for uncovering the molecular mechanisms behind these interactions and observations. Until this is known, it will not be possible to fully understand these pathways or find ways to target them in order to treat the associated diseases.

Acknowledgments

The author wishes to thank Dr. Shantá D. Hinton for her guidance and support. The author also wishes to thank Lynn Zavada for her contributions to this project. Additionally, the author would like to thank Dr. Martin Safo and Dr. Faik Musayev of the VCU School of Pharmacy's Institute for Structural Biology, Drug Discovery and Development. The author would like to give special thanks to the Virginia Space Grant Consortium for their financial support. This work was also supported by the National Science Foundation Grant MCB1909316 to S.D.H.

References

(1) Hinton, S. D. The Role of Pseudophosphatases as Signaling Regulators. *Biochimica et Biophysica Acta (BBA) - Molecular Cell Research* **2019**, *1866* (1), 167–174. https://doi.org/10.1016/j.bbamcr.2018.07.021.

(2) Protein Kinases and Phosphatases: The Yin and Yang of Protein Phosphorylation and Signaling. *Cell* **1995**, *80* (2), 225–236. https://doi.org/10.1016/0092-8674(95)90405-0.
(3) Murphy, J. M.; Farhan, H.; Eyers, P. A. Bio-Zombie: The Rise of Pseudoenzymes in Biology. *Biochem Soc Trans* **2017**, *45* (2), 537–544. https://doi.org/10.1042/BST20160400.
(4) Todd, A. E.; Orengo, C. A.; Thornton, J. M. Sequence and Structural Differences between Enzyme and Nonenzyme Homologs. *Structure* **2002**, *10* (10), 1435–1451. https://doi.org/10.1016/S0969-2126(02)00861-4.
(5) Murphy, J. M.; Mace, P. D.; Eyers, P. A. Live and Let Die: Insights into Pseudoenzyme Mechanisms from Structure. *Current Opinion in Structural Biology* **2017**, *47*, 95–104. https://doi.org/10.1016/j.sbi.2017.07.004.
(6) Reiterer, V.; Eyers, P. A.; Farhan, H. Day of the Dead: Pseudokinases and Pseudophosphatases in Physiology and Disease. *Trends in Cell Biology* **2014**, *24* (9), 489–505. https://doi.org/10.1016/j.tcb.2014.03.008.
(7) Reiterer, V.; Pawłowski, K.; Desrochers, G.; Pause, A.; Sharpe, H. J.; Farhan, H. The Dead Phosphatases Society: A Review of the Emerging Roles of Pseudophosphatases. *The FEBS Journal* **2020**, *287* (19), 4198–4220. https://doi.org/10.1111/febs.15431.
(8) Tonks, N. K. Pseudophosphatases: Grab and Hold On. *Cell* **2009**, *139* (3), 464–465. https://doi.org/10.1016/j.cell.2009.10.008.
(9) Hinton, S. D.; Myers, M. P.; Roggero, V. R.; Allison, L. A.; Tonks, N. K. The Pseudophosphatase MK-STYX Interacts with G3BP and Decreases Stress Granule Formation. *Biochem J* **2010**, *427* (Pt 3), 349–357. https://doi.org/10.1042/BJ20091383.
(10) Hinton, S. D. Pseudophosphatase MK-STYX: The Atypical Member of the MAP Kinase Phosphatases. *The FEBS Journal* **2020**, *287* (19), 4221–4231. https://doi.org/10.1111/febs.15426.
(11) Niemi, N. M.; MacKeigan, J. P. MK-STYX. In *Encyclopedia of Signaling Molecules*; Choi, S., Ed.; Springer: New York, NY, 2012; pp 1089–1093. https://doi.org/10.1007/978-1-4419-0461-4_205.
(12) Caunt, C. J.; Keyse, S. M. Dual-Specificity MAP Kinase Phosphatases (MKPs). *The FEBS Journal* **2013**, *280* (2), 489–504. https://doi.org/10.1111/j.1742-4658.2012.08716.x.
(13) Farooq, A.; Chaturvedi, G.; Mujtaba, S.; Plotnikova, O.; Zeng, L.; Dhalluin, C.; Ashton, R.; Zhou, M.-M. Solution Structure of ERK2 Binding Domain of MAPK Phosphatase MKP-3: Structural Insights into MKP-3 Activation by ERK2. *Molecular Cell* **2001**, *7* (2), 387–399. https://doi.org/10.1016/S1097-2765(01)00186-1.
(14) Nichols, A.; Camps, M.; Gillieron, C.; Chabert, C.; Brunet, A.; Wilsbacher, J.; Cobb, M.; Pouyssegur, J.; Shaw, J. P.; Arkinstall, S. Substrate Recognition Domains within Extracellular Signal-Regulated Kinase Mediate Binding and Catalytic Activation of Mitogen-Activated Protein Kinase Phosphatase-3. *J. Biol. Chem.* **2000**, *275* (32), 24613–24621. https://doi.org/10.1074/jbc.M001515200.
(15) Tonks, N. K. Protein Tyrosine Phosphatases: From Genes, to Function, to Disease. *Nat. Rev. Mol. Cell Biol.* **2006**, *7* (11), 833–846. https://doi.org/10.1038/nrm2039.
(16) Tonks, N. K. Special Issue: Protein Phosphatases: From Molecules to Networks. *The FEBS Journal* **2013**, *280* (2), 323–323. https://doi.org/10.1111/febs.12098.
(17) Tonks, N. K. Protein Tyrosine Phosphatases – from Housekeeping Enzymes to Master Regulators of Signal Transduction. *The FEBS Journal* **2013**, 346–378. https://doi.org/10.1111/febs.12077
(18) Tonks, N. K.; Neel, B. G. Combinatorial Control of the Specificity of Protein Tyrosine Phosphatases. *Current Opinion in Cell Biology* **2001**, *13* (2), 182–195. https://doi.org/10.1016/S0955-0674(00)00196-4.
(19) Reiterer, V.; Pawłowski, K.; Farhan, H. STYX: A Versatile Pseudophosphatase. *Biochem Soc Trans* **2017**, *45* (2), 449–456. https://doi.org/10.1042/BST20160279.
(20) Wishart, M. J.; Dixon, J. E. Gathering STYX: Phosphatase-like Form Predicts Functions for Unique Protein-Interaction Domains. *Trends in Biochemical Sciences* **1998**, *23* (8), 301–306. https://doi.org/10.1016/S0968-0004(98)01241-9.
(21) Wishart, M. J.; Denu, J. M.; Williams, J. A.; Dixon, J. E. A Single Mutation Converts a Novel Phosphotyrosine Binding Domain into a Dual-Specificity Phosphatase. *J. Biol. Chem.* **1995**, *270* (45), 26782–26785. https://doi.org/10.1074/jbc.270.45.26782.
(22) Stewart, A. E.; Dowd, S.; Keyse, S. M.; McDonald, N. Q. Crystal Structure of the MAPK Phosphatase Pyst1 Catalytic Domain and Implications for Regulated Activation. *Nat. Struct. Biol.* **1999**, *6* (2), 174–181. https://doi.org/10.1038/5861.
(23) Niemi, N. M.; Lanning, N. J.; Klomp, J. A.; Tait, S. W.; Xu, Y.; Dykema, K. J.; Murphy, L. O.; Gaither, L. A.; Xu, H. E.; Furge, K. A.; et al. MK-STYX, a Catalytically Inactive Phosphatase Regulating Mitochondrially Dependent Apoptosis. *Molecular and Cellular Biology* **2011**, *31* (7), 1357–1368. https://doi.org/10.1128/MCB.00788-10.
(24) Niemi, N. M.; Sacoman, J. L.; Westrate, L. M.; Gaither, L. A.; Lanning, N. J.; Martin, K. R.; MacKeigan, J. P. The Pseudophosphatase MK-STYX Physically and Genetically Interacts with the Mitochondrial Phosphatase PTPMT1. *PLoS One; San Francisco* **2014**, *9* (4), e93896. http://dx.doi.org/10.1371/journal.pone.0093896.
(25) Tomar, V. S.; Baral, T. K.; Nagavelu, K.; Somasundaram, K. Serine/Threonine/Tyrosine-Interacting-like Protein 1 (STYXL1), a Pseudo Phosphatase, Promotes Oncogenesis in Glioma. *Biochemical and Biophysical Research Communications* **2019**, *515* (1), 241–247. https://doi.org/10.1016/j.bbrc.2019.05.093.
(26) J. Z. Wu; N Jiang; J. M. Lin; X. Liu. STYXL1 Promotes Malignant Progression of Hepatocellular Carcinoma via Downregulating CELF2 through the PI3K/Akt Pathway. *European Review* **2020**, *24* (6), 2977–2985. https://doi.org/10.26355/eurrev_202003_20662.
(27) Banks, D. A.; Dahal, A.; McFarland, A. G.; Flowers, B. M.; Stephens, C. A.; Swack, B.; Gugssa, A.; Anderson, W. A.; Hinton, S. D. MK-STYX Alters the Morphology of Primary Neurons, and Outgrowths in MK-STYX Overexpressing PC-12 Cells Develop a Neuronal Phenotype. *Front Mol Biosci* **2017**, *4*. https://doi.org/10.3389/fmolb.2017.00076.
(28) Dahal, A.; Hinton, S. D. Antagonistic Roles for STYX Pseudophosphatases in Neurite Outgrowth. *Biochemical Society Transactions* **2017**, *45* (2), 381–387. https://doi.org/10.1042/BST20160273.
(29) Flowers, B. M.; Rusnak, L. E.; Wong, K. E.; Banks, D. A.; Munyikwa, M. R.; McFarland, A. G.; Hinton, S. D. The Pseudophosphatase MK-STYX Induces Neurite-Like Outgrowths in PC12 Cells. *PLoS One* **2014**, *9* (12). https://doi.org/10.1371/journal.pone.0114535.
(30) Isrie, M.; Zamani Esteki, M.; Peeters, H.; Voet, T.; Van Houdt, J.; Van Paesschen, W.; Van Esch, H. Homozygous Missense Mutation in STYXL1 Associated with Moderate Intellectual Disability, Epilepsy and Behavioural Complexities. *European Journal of Medical Genetics* **2015**, *58* (4), 205–210. https://doi.org/10.1016/j.ejmg.2015.02.006.
(31) Youn, J.-Y.; Dyakov, B. J. A.; Zhang, J.; Knight, J. D. R.; Vernon, R. M.; Forman-Kay, J. D.; Gingras, A.-C. Properties of Stress Granule and P-Body Proteomes. *Molecular Cell* **2019**, *76* (2), 286–294. https://doi.org/10.1016/j.molcel.2019.09.014.
(32) Protter, D. S. W.; Parker, R. Principles and Properties of Stress Granules. *Trends in Cell Biology* **2016**, *26* (9), 668–679. https://doi.org/10.1016/j.tcb.2016.05.004.

(33) Barr, J. E.; Munyikwa, M. R.; Frazier, E. A.; Hinton, S. D. The Pseudophosphatase MK-STYX Inhibits Stress Granule Assembly Independently of Ser149 Phosphorylation of G3BP-1. *The FEBS Journal* **2013**, *280* (1), 273–284. https://doi.org/10.1111/febs.12068.

(34) Guillén-Boixet, J.; Kopach, A.; Holehouse, A. S.; Wittmann, S.; Jahnel, M.; Schlüßler, R.; Kim, K.; Trussina, I. R. E. A.; Wang, J.; Mateju, D.; et al. RNA-Induced Conformational Switching and Clustering of G3BP Drive Stress Granule Assembly by Condensation. *Cell* **2020**, *181* (2), 346-361.e17. https://doi.org/10.1016/j.cell.2020.03.049.

(35) Nemoto, S.; Ohnuki, S.; Abe, F.; Ohya, Y. Simulated Microgravity Triggers Characteristic Morphology and Stress Response in Saccharomyces Cerevisiae. *Yeast* **2019**, *36* (2), 85–97. https://doi.org/10.1002/yea.3361.

(36) Graebe, A.; Schuck, E. L.; Lensing, P.; Putcha, L.; Derendorf, H. Physiological, Pharmacokinetic, and Pharmacodynamic Changes in Space. *The Journal of Clinical Pharmacology* **2004**, *44* (8), 837–853. https://doi.org/10.1177/0091270004267193.

(37) Qu, L.; Chen, H.; Liu, X.; Bi, L.; Xiong, J.; Mao, Z.; Li, Y. Protective Effects of Flavonoids Against Oxidative Stress Induced by Simulated Microgravity in SH-SY5Y Cells. *Neurochem Res* **2010**, *35* (9), 1445–1454. https://doi.org/10.1007/s11064-010-0205-4.

(38) Zhao, L.; Rui, Q.; Wang, D. Molecular Basis for Oxidative Stress Induced by Simulated Microgravity in Nematode Caenorhabditis Elegans. *Science of The Total Environment* **2017**, *607–608*, 1381–1390. https://doi.org/10.1016/j.scitotenv.2017.07.088.

(39) Hinton, S. D. Analyzing Pseudophosphatase Function. In *Protein Tyrosine Phosphatases: Methods and Protocols*; Pulido, R., Ed.; Methods in Molecular Biology; Springer: New York, NY, 2016; pp 139–153. https://doi.org/10.1007/978-1-4939-3746-2_9.

(40) Gumpena, R.; Lountos, G. T.; Raran-Kurussi, S.; Tropea, J. E.; Cherry, S.; Waugh, D. S. Crystal Structure of the Human Dual Specificity Phosphatase 1 Catalytic Domain. *Protein Sci.* **2018**, *27* (2), 561–567. https://doi.org/10.1002/pro.3328.

(41) Callaway, E. Revolutionary Cryo-EM Is Taking over Structural Biology. *Nature* **2020**, *578*, 201–201. https://doi.org/10.1038/d41586-020-00341-9.

(42) Liu, H.-L.; Hsu, J.-P. Recent Developments in Structural Proteomics for Protein Structure Determination. *PROTEOMICS* **2005**, *5* (8), 2056–2068. https://doi.org/10.1002/pmic.200401104.

(43) Berman, H. M.; Westbrook, J.; Feng, Z.; Gilliland, G.; Bhat, T. N.; Weissig, H.; Shindyalov, I. N.; Bourne, P. E. The Protein Data Bank. *Nucleic Acids Res* **2000**, *28* (1), 235–242. https://doi.org/10.1093/nar/28.1.235.

(44) Wlodawer, A.; Minor, W.; Dauter, Z.; Jaskolski, M. Protein Crystallography for Non-Crystallographers, or How to Get the Best (but Not More) from Published Macromolecular Structures. *FEBS J* **2008**, *275* (1), 1–21. https://doi.org/10.1111/j.1742-4658.2007.06178.x.

(45) Almo, S. C.; Bonanno, J. B.; Sauder, J. M.; Emtage, S.; Dilorenzo, T. P.; Malashkevich, V.; Wasserman, S. R.; Swaminathan, S.; Eswaramoorthy, S.; Agarwal, R.; et al. Structural Genomics of Protein Phosphatases. *J Struct Funct Genomics* **2007**, *8* (2), 121–140. https://doi.org/10.1007/s10969-007-9036-1.

(46) Bilotta, M.; Tradigo, G.; Veltri, P. Bioinformatics Data Models, Representation and Storage. In *Encyclopedia of Bioinformatics and Computational Biology*; Ranganathan, S., Gribskov, M., Nakai, K., Schönbach, C., Eds.; Academic Press: Oxford, 2019; pp 110–116. https://doi.org/10.1016/B978-0-12-809633-8.20410-X.

(47) Luscombe, N. M.; Greenbaum, D.; Gerstein, M. What Is Bioinformatics? A Proposed Definition and Overview of the Field. *Methods Inf Med* **2001**, *40* (04), 346–358. https://doi.org/10.1055/s-0038-1634431.

(48) Korneta, I.; Magnus, M.; Bujnicki, J. M. Structural Bioinformatics of the Human Spliceosomal Proteome. *Nucleic Acids Res* **2012**, *40* (15), 7046–7065. https://doi.org/10.1093/nar/gks347.

(49) Nithin, C.; Ghosh, P.; Bujnicki, J. M. Bioinformatics Tools and Benchmarks for Computational Docking and 3D Structure Prediction of RNA-Protein Complexes. *Genes* **2018**, *9* (9), 432. https://doi.org/10.3390/genes9090432.

(50) *Structural Bioinformatics*, 1st ed.; John Wiley & Sons, Ltd, 2003. https://doi.org/10.1002/0471721204.

(51) Gauthier, J.; Vincent, A. T.; Charette, S. J.; Derome, N. A Brief History of Bioinformatics. *Brief Bioinform* **2019**, *20* (6), 1981–1996. https://doi.org/10.1093/bib/bby063.

(52) Gupta, C. L.; Akhtar, S.; Bajpai, P. In Silico Protein Modeling: Possibilities and Limitations. *EXCLI J* **2014**, *13*, 513–515.

(53) Yang, J.; Zhang, Y. I-TASSER Server: New Development for Protein Structure and Function Predictions. *Nucleic Acids Res* **2015**, *43* (W1), W174–W181. https://doi.org/10.1093/nar/gkv342.

(54) Yang, J.; Yan, R.; Roy, A.; Xu, D.; Poisson, J.; Zhang, Y. The I-TASSER Suite: Protein Structure and Function Prediction. *Nature Methods; New York* **2015**, *12* (1), 7–8. http://dx.doi.org/10.1038/nmeth.3213.

(55) Zhang, C.; Freddolino, P. L.; Zhang, Y. COFACTOR: Improved Protein Function Prediction by Combining Structure, Sequence and Protein-Protein Interaction Information. *Nucleic Acids Res* **2017**, *45* (W1), W291–W299. https://doi.org/10.1093/nar/gkx366.

(56) Wise, M. C. ISB3D X-Ray Crystallography Facility. 5.

(57) Chen, V. B.; Arendall, W. B.; Headd, J. J.; Keedy, D. A.; Immormino, R. M.; Kapral, G. J.; Murray, L. W.; Richardson, J. S.; Richardson, D. C. MolProbity: All-Atom Structure Validation for Macromolecular Crystallography. *Acta Crystallogr D Biol Crystallogr* **2010**, *66* (Pt 1), 12–21. https://doi.org/10.1107/S0907444909042073.

(58) Davis, I. W.; Leaver-Fay, A.; Chen, V. B.; Block, J. N.; Kapral, G. J.; Wang, X.; Murray, L. W.; Arendall, W. B.; Snoeyink, J.; Richardson, J. S.; et al. MolProbity: All-Atom Contacts and Structure Validation for Proteins and Nucleic Acids. *Nucleic Acids Res* **2007**, *35* (Web Server issue), W375-383. https://doi.org/10.1093/nar/gkm216.

(59) Williams, C. J.; Headd, J. J.; Moriarty, N. W.; Prisant, M. G.; Videau, L. L.; Deis, L. N.; Verma, V.; Keedy, D. A.; Hintze, B. J.; Chen, V. B.; et al. MolProbity: More and Better Reference Data for Improved All-Atom Structure Validation. *Protein Sci* **2018**, *27* (1), 293–315. https://doi.org/10.1002/pro.3330.

(60) Yu, J.; Zhou, Y.; Tanaka, I.; Yao, M. Roll: A New Algorithm for the Detection of Protein Pockets and Cavities with a Rolling Probe Sphere. *Bioinformatics* **2010**, *26* (1), 46–52. https://doi.org/10.1093/bioinformatics/btp599.

(61) *The PyMOL Molecular Graphics System, Version 2.0 Schrödinger, LLC.*